Received: 15 March 2021 | Revised: 18 December 2021 | Accepted: 1 January 2022

DOI: 10.1002/dac.5094

RESEARCH ARTICLE

WILEY

A novel orthogonal frequency division multiplexing with index modulation waveform with carrier frequency offset resistance and low peak-to-average power ratio

Ilter Erol Gurol[1] | **Ertugrul Basar**[1] | **Defne Kucukyavuz**[2] | **Furuzan Atay Onat**[2]

[1]Communications Research and Innovation Laboratory (CoreLab), Department of Electrical and Electronics Engineering, Koç University, Istanbul, Turkey

[2]HBT, ASELSAN A.S., Ankara, Turkey

Correspondence
Ilter Erol Gurol, Department of Electrical and Electronics Engineering, Koç University, Istanbul, Turkey.
Email: igurol19@ku.edu.tr

Funding information
ASELSAN A.S., Grant/Award Number: HBT-TE-2019-010

Summary

In this paper, we propose a novel orthogonal frequency division multiplexing (OFDM) scheme with high carrier frequency offset (CFO) resistance and low peak-to-average power ratio (PAPR). In this scheme, we consider a hybrid model with two subblock types, namely, pilot subblocks and standard subblocks. In pilot subblocks, active subcarriers are utilized for PAPR reduction while inactive carriers generated by the index modulation (IM) are utilized for the coarse CFO estimation. For standard subblocks, we consider unique subcarrier activation patterns (SAPs) with high-diversity IM to enhance the bit error performance of the overall system. Additionally, the inactive data tones in standard subblocks are utilized for fine CFO estimation, which enhances the CFO estimation quite significantly. Furthermore, in this paper, we show that proposed hybrid OFDM-IM (H-OFDM-IM) scheme can outperform conventional OFDM-IM and classical OFDM both in CFO estimation and PAPR reduction without requiring transmission of any side information. Finally, we show both mathematically and through computer simulations that proposed H-OFDM-IM can achieve a satisfactory bit error rate (BER) performance under high CFO scenarios.

KEYWORDS

carrier frequency offset (CFO), orthogonal frequency division multiplexing with index modulation (OFDM-IM), peak-to-average power ratio (PAPR)

1 | INTRODUCTION

Orthogonal frequency division multiplexing with index modulation (OFDM-IM) is a highly attractive technique for high rate data transmission under multipath and frequency-selective wireless channels due to its resistance against intersymbol interference (ISI) and improved performance compared to classical OFDM.[1–4] However, OFDM-based systems are relatively sensitive to the carrier frequency offset (CFO), which is caused by frequency mismatches between the transmitter and receiver or by Doppler effect.[5] To achieve reliable communication, intercarrier interference (ICI) caused by the CFO must be estimated and compensated.[6] Moreover, high peak-to-average power ratio (PAPR) at the transmitter side either limits the efficiency of high-power amplifiers (HPAs) by forcing them to operate in linear region or causes HPAs to operate in nonlinear region, disturbing the time-domain OFDM signal.[7] These undesired distortions cause high bit error rate (BER) at the receiver and degrade the overall system

performance. Since CFO, PAPR, and BER performance are the three main aspects and concerns of a multicarrier-based communication system, it becomes a big challenge to design adaptive systems, which can efficiently overcome these in dynamic environments.

Frequency-selective fading channels with high mobility terminals cause frequency mismatch between the transmitter and the receiver.[8] Various methods and algorithms are proposed for the CFO estimation. Several blind CFO estimation algorithms are given in previous studies.[5,9–12] Although blind CFO estimation techniques do not decrease the spectral efficiency of a given system, they suffer from imprecise CFO estimations. In Mokhtar et al,[13] a semiblind CFO estimation technique is considered, which utilizes zero pilots. Another CFO estimation process proposes transmitting training sequences at the beginning of each frame.[14] However, training sequence-based CFO estimation techniques degrade the efficiency of the communication system and require multiple OFDM symbols to be effective. An analysis for joint CFO and channel estimation design for OFDM systems are given in Lin and Hwang.[15] A fundamentally different approach in Ma et al[16] uses null subcarriers in OFDM to estimate the CFO. In Yang et al,[17] it is shown that a similar idea can be implemented in OFDM with generalized index modulation (OFDM-GIM). Using null subcarrier-based CFO estimation techniques in OFDM-IM systems increases the system efficiency, since it utilizes the inactive data tones generated by the IM. However, the method in Yang et al[17] has degraded performance under low signal-to-noise-ratio (SNR) conditions due to threshold and power-based estimation methodologies.

Another big concern of an OFDM-based communication system is high PAPR. OFDM-IM, in this case, has several advantages compared to classical OFDM. Due to its inactive data tones, OFDM-IM requires less power and has a lower PAPR in comparison to the classical OFDM. The two well-known PAPR reduction algorithms, partial transmit sequence (PTS) and selective mapping (SLM), which require transmission of side information, are given in Wang et al[18] and Liang.[19] Although there are some special versions of PTS and SLM, which do not require any side information, conventional PTS and SLM algorithms require this information to be sent. In Thota et al,[20] a comparison between classical and hybrid PAPR reduction methodologies are presented. A colony optimization-based PAPR reduction approach is presented in Hosseinzadeh Aghdam and Sharifi.[21] Another different approach, which utilizes the interesting concept of active constellation extension (ACE), is given in Memisoglu et al.[22] ACE, in comparison to classical methodologies, offers higher spectral efficiency. However, ACE method increases the average constellation symbol power to balance the PAPR. However, this may cause further problems in some applications.

In this paper, we proposed a resilient multicarrier waveform based on OFDM-IM structure for a self-organizing mobile ad hoc communication network where the transmissions are intermittent, the transmitter and receiver pairs change frequently, and the channel is time varying requiring the CFO estimation to be performed and compensated within the same multicarrier symbol carrying the information bits. The proposed waveform utilizes the diversity provided by index modulation for robust and spectrally efficient transmission of the critical information essential for demodulation of the multicarrier symbol (e.g., coding rate and modulation order) that is typically carried in the header field of the frame in contemporary communication standards. The proposed novel hybrid OFDM-IM (H-OFDM-IM) waveform additionally addresses the CFO estimation and PAPR reduction problem of multicarrier modulations such as OFDM.

The proposed H-OFDM-IM system takes both CFO and PAPR problem of OFDM systems into account and embeds two different types of subblocks (pilot and standard subblocks) into one H-OFDM-IM symbol to perform an accurate estimation of CFO and overcome the high PAPR problem without the transmission of any side information. To coarsely estimate the CFO, we consider utilizing the null subcarriers in the pilot subblocks, in which the active subcarriers in the very same subblocks are used for the minimization of the PAPR. To further enhance the CFO estimation, we consider utilizing all of the inactive data tones in an H-OFDM-IM symbol for fine CFO estimation. Moreover, with extensive computer simulations and mathematical derivations, we show that a precise estimation and compensation of CFO can be performed to overcome ICI, while reducing the PAPR of the H-OFDM-IM symbol in a low-complex way and with minimal sacrifice in the spectral efficiency.

Furthermore, our novel system is capable of adjusting the diversity of bits carried by IM so that H-OFDM-IM symbol can be optimized for different use cases. These use cases may target a specific spectral efficiency or may require high BER performance for certain critical bits, which may be necessary to demodulate the entire H-OFDM-IM symbol. To show the robustness of proposed system, we investigate the performance of the proposed H-OFDM-IM scheme with LDPC channel coding under high CFO conditions and compare them with the results with conventional OFDM-IM

and classical OFDM. Our extensive computer simulations show that our new waveform can achieve lower mean square error (MSE) values for CFO estimation and can efficiently decrease PAPR while providing satisfactory spectral efficiency for various SNR conditions.

2 | SYSTEM MODEL

In this section, we provide the mathematical model for the proposed H-OFDM-IM symbol. First, we derive the mathematical model for proposed H-OFDM-IM symbol; then, we explain the low-complexity PAPR reduction algorithm, followed by coarse and fine CFO estimation and compensation. Finally, we explain how the SNR estimation is performed based on the residual power on estimated inactive data tones.

2.1 | H-OFDM-IM symbol structure

In the proposed hybrid OFDM-IM (H-OFDM-IM) system, we consider an OFDM-IM symbol with N subcarriers and $g = \frac{N}{n}$ subblocks, where a subblock consists of n subcarriers. Proposed H-OFDM-IM symbol consists of two different types of subblocks as shown in Figure 1. From g subblocks, we define g_p of them to be pilot subblocks and g_s to be standard OFDM-IM subblocks with special subcarrier activation patterns (SAPs). These equally spaced pilot subblocks are responsible for coarse CFO estimation and PAPR reduction of a given H-OFDM-IM symbol and do not carry any information. Additionally, these pilot subblocks have a predetermined number of pilot tones, where k_p is a waveform parameter. In Figure 1, case of $k_p = \frac{n}{2}$ is depicted. These pilot data tones are suggested to be equally spaced among the pilot subblock for maximum frequency diversity and minimal ICI.

The standard H-OFDM-IM subblocks are mainly used for data transmission. However, the inactive data tones in these standard subbblocks are indirectly used for the fine CFO estimation as well. In these standard subblocks, we set the number of active subcarriers to be $k_s \in \{\frac{n}{2}, \frac{n}{4}, ..., 2\}$ and to be compatible with the special high-diversity IM scheme. Selection of k_s depends on the application requirements, and it directly determines the IM diversity gain. Furthermore, in these subblocks, we enforce special SAPs depending on k_s, so that a better BER performance through increased diversity can be achieved. These high-diversity SAPs do not have any intersecting subcarrier indices in a given subblock and

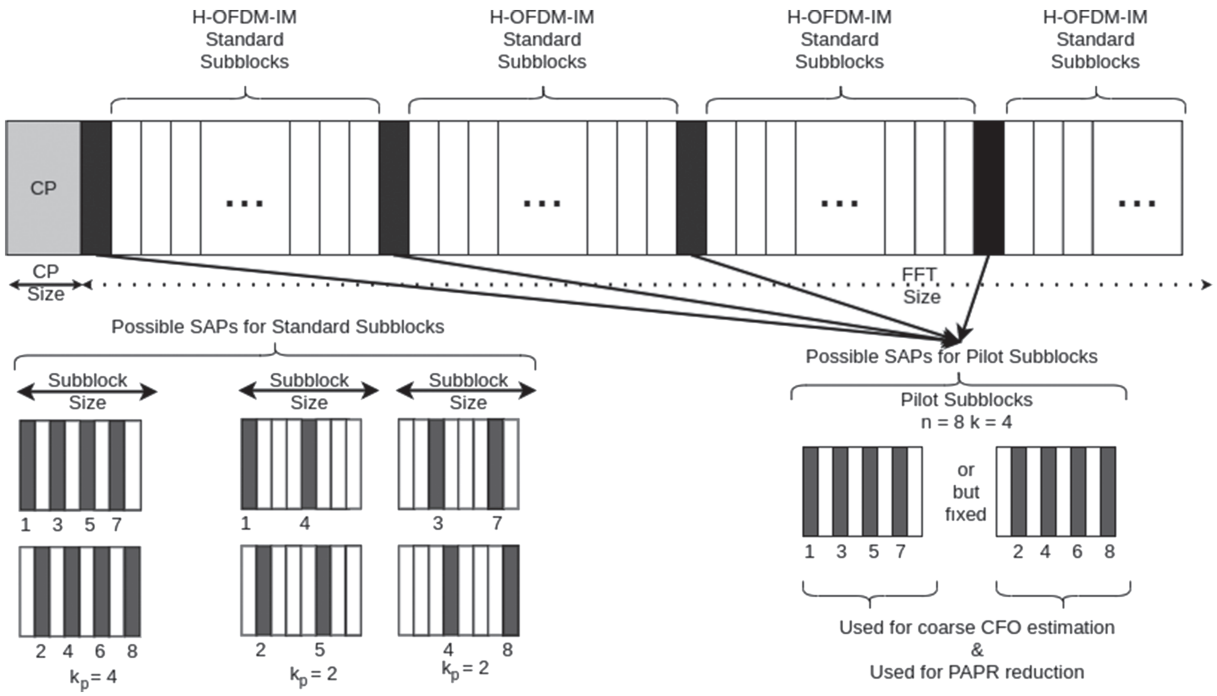

FIGURE 1 H-OFDM-IM symbol structure

TABLE 1 SAPs of the proposed OFDM-IM system depending on the selected k_p

k_s	Possible SAPs for standard subblocks
2	$\{\{1,5\},\{2,6\},\{3,7\},\{4,8\}\}$
4	$\{\{1,3,5,7\},\{2,4,6,8\}\}$

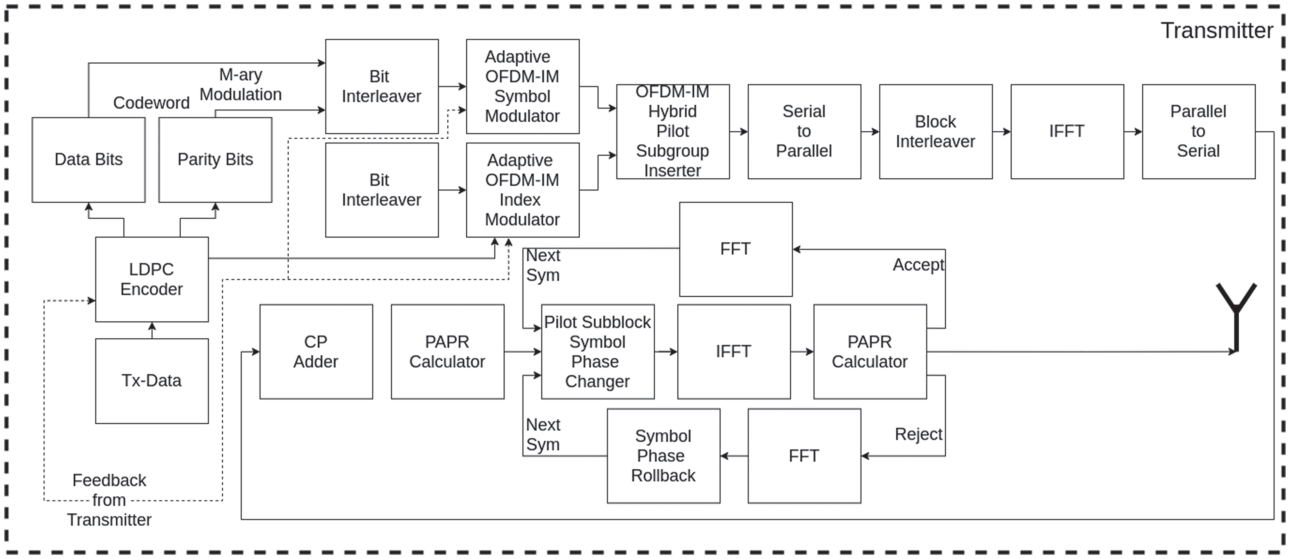

FIGURE 2 H-OFDM-IM transmitter structure

therefore are more error prone to bit errors carried over IM. For $n = 8$, examples of high-diversity SAPs are given in Table 1, where the diversity gain is set to be 4 for $k_s = 4$ and 2 for $k_s = 2$.

With the nonoverlapping SAP structures (i.e., for $n = 8$ given in Table 1), we construct the unique IM structure of standard subblocks with respect to the input information and modulate the active carriers in these subblocks with respect to the selected modulation scheme and information. Moreover, we set k_p of n subcarriers in pilot subblocks to be active. For optimal CFO estimation performance and PAPR reduction, we consider spreading the active subcarriers equally among the subblock. In similar fashion, for increased diversity, we consider equally spaced pilot subblocks throughout an H-OFDM-IM symbol as shown in Figure 1. However, for increased PAPR reduction, one can select $k_p \leq n$ by sacrificing coarse CFO estimation accuracy. An increase in the number of pilot subblocks g_p contributes to both coarse CFO estimation and PAPR reduction in expense of spectral efficiency. Here, it is also important to note that the time synchronization could be not be directly achieved with such a structure, and classical approach of using a preamble symbol for frame synchronization can be still used. However, in this paper, we oriented our focus on the CFO estimation, which could change frequently in the dynamic environments.

When we analyze the waveform and the number of bits transmitted, we can see that in a single standard subblock, we can transmit $b_s = \log_2(p) + k_s \times \log_2 M$ bits, where p denotes the number of possible SAPs for the selected k_s. Overall, we have $K = g_s \times k_s + g_p \times k_p$ active subcarriers in an H-OFDM-IM symbol, over which we can transmit $b = g_s \times b_s$ bits. From those b bits, $b_{IM} = g_s \times \log_2 p$ bits are transmitted with IM and $b_M = g_s \times k_s \times \log_2 M$ bits are transmitted with the modulation of $g_s \times k_s$ active subcarriers, where $K - g_s \times k_s$ subcarriers are used for PAPR reduction.

The set of K active subcarriers' indices are represented with $\mathcal{A}$, where $\mathcal{A}_p \subset \mathcal{A}$ is the set of active subcarriers in pilot subblocks, and $\mathcal{A}_s \subset \mathcal{A}$ is the set of indices of the active data tones in standard subblocks. In a similar fashion, we define the indices of all inactive data tones as $\mathcal{Z}$, where $\mathcal{Z}_p, \mathcal{Z}_s \subset \mathcal{Z}$ are the inactive data tones of pilot subblocks and standard subblocks, respectively.

By following the transmitter design in Figure 2 to construct the H-OFDM-IM symbol in Figure 1 with optimal PAPR, we encode the transmit data of length m_r with LDPC (a forward error correction technique also used in 5G systems to provide superior error correction capability). After encoding the transmit data, we split m_d encoded data bits and m_p parity bits in the codeword of length $m_c = m_d + m_p$ and feed forward to bit-level interleavers, so that data bits and parity bits generated by LDPC channel coding can be interleaved. As a result, bit-level interleaving provides a slight improvement in BER performance of the system. Since we perform two different modulation techniques on proposed H-OFDM-IM symbol, we need two different types of modulators at the transmitter. The first one is responsible for the IM of critical bits. The second modulator modulates the active data tones in the H-OFDM-IM symbol. For modulation of the active subcarriers, we consider M-ary modulation schemes and select the modulation scheme with respect to the feedback information.

The constructed H-OFDM-IM symbol after IM and the modulation of active subcarriers can be denoted as $\{\overline{x}(l)\}_{l=1}^{N}$, where $\overline{x}(l)$ is the lth frequency component. These frequency components are then passed through a block interleaver (with row size g and column size n) to maximize the frequency diversity among the subcarriers in a single subblock. The maximized frequency diversity among the subcarriers in a subblock minimizes the BER in IM and indirectly improves the fine CFO estimation as well. The signal after block interleaving can be represented as $\{\hat{x}(l)\}_{l=1}^{N}$, while $\mathcal{A}'$ and $\mathcal{Z}'$ denote the sets of active data tones and inactive data tones, respectively. Similarly, we denote $\mathcal{A}'_s, \mathcal{A}'_p, \mathcal{Z}'_s$, and $\mathcal{Z}'_p$ after the block interleaving.

At this stage in the transmitter, we perform N-point inverse fast Fourier transform (IFFT) on $\hat{\mathbf{x}}$: $\underline{\mathbf{x}} = \frac{N}{\sqrt{K}}\text{IFFT}\{\hat{\mathbf{x}}\} = \frac{1}{\sqrt{K}}\mathbf{F}_N^H\hat{\mathbf{x}}$ where $\underline{\mathbf{x}}$ is the time-domain representation of the signal. Here, $\mathbf{F}_N$ is the discrete Fourier transform (DFT) matrix with $\mathbf{F}_N^H\mathbf{F}_N = N\mathbf{I}_N$, and the term $\frac{N}{\sqrt{K}}$ is used for the normalization $E\{\underline{\mathbf{x}}^H\underline{\mathbf{x}}\} = N$. Then, to minimize ICI, we add cyclic prefix (CP) of length L.

Algorithm 1 Greedy PAPR reduction

```
N, A_p, g_p, k_p, g_p, q x
A_p ∉ ∅, N ≠ 0
i ← 0
x_new ← x                                   ▷ Start from the first active data tone in Pilot subblocks
while i < g_p × k_p do
    l ← 0                                   ▷ Iterate over possible phase shifts
    while l < q do
        x_new(d_i) ← x_new(d_i) · exp(j2π/l)
        if PAPR{x} > PAPR{x_new} then
            x ← x_new                       ▷ New OFDM-IM symbol
        else
            x_new(d_i) ← x_new(d_i) · exp((−1)j2π/l)   ▷ Remove phase shift
        end if
    end while
end while
return x
```

Once, the H-OFDM-IM symbol is complete, we continue with the PAPR reduction. Proposed PAPR reduction algorithm avoids transmission of any form of side information by modulating the active data tone indices $\mathcal{A}_p$ with dummy PSK symbols and phase shifting them. Let us denote these dummy symbols with $d_0, d_1, ..., d_{g_p \times k_p}$. Starting from the first dummy symbol d_0, we multiply each d_i with discrete phase factors vector $\mathbf{q} = [\exp(\frac{j2\pi}{q}), \exp(\frac{j2\pi}{q-1}), ...\exp(\frac{j2\pi}{1})]^T$, where $i \in \{0, 1, ..., d_{g_p \times k_p}\}$ and $q \in \mathbb{Z}^+$ and defines the resolution. Then, for each element of $d_i \times \mathbf{q}$ vector, we perform N-point IFFT and calculate

$$\text{PAPR}\{\underline{\mathbf{x}}\} = \frac{\max_i |\underline{\mathbf{x}}|^2}{E\{|\underline{\mathbf{x}}|^2\}}, \tag{1}$$

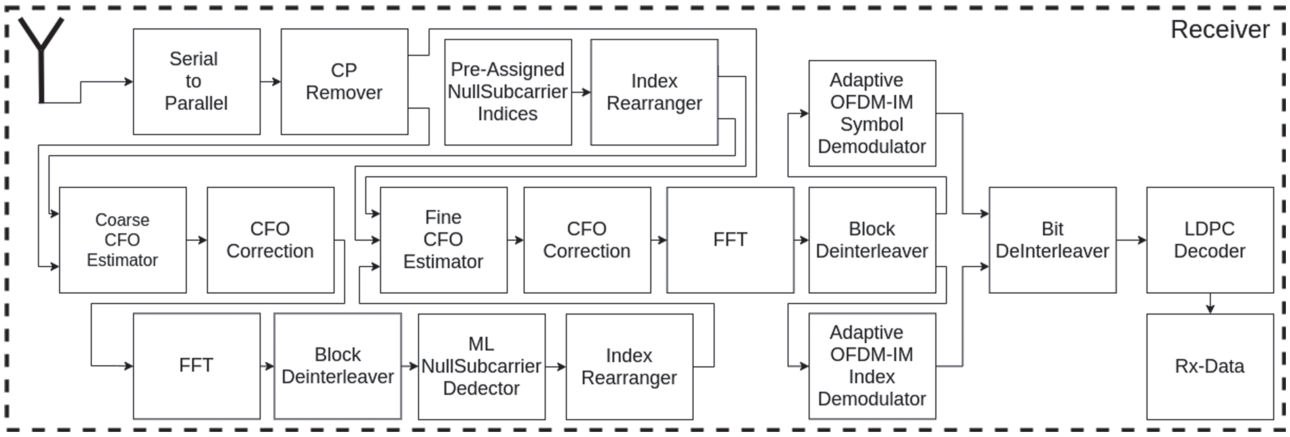

FIGURE 3 H-OFDM-IM receiver structure

where $\iota = 0,1,...,N-1$ and $\underline{\mathbf{x}}$ defines the time-domain samples of the signal. At this stage, we select the $\min_{d_i \times \mathbf{q}} PAPR\{\underline{\mathbf{x}}\}$ for PAPR reduction on d_i dummy symbol. Once all PAPR values for each d_ith dummy symbol is calculated, the greedy PAPR reduction on a H-OFDM-IM symbol is complete. The performed greedy algorithm for minimizing PAPR of a given H-OFDM-IM symbol can be seen in Algorithm 1. Definitely, we get a suboptimal result by using a greedy algorithm. However, such an algorithm keeps the complexity at minimum and avoids processing $C(g_p \times k_p \times \dim(q), g_p \times k_p) = \frac{(g_p \times k_p \times dim(q))!}{(g_p \times k_p)!((\dim(q)-1) \times g_p \times k_p)!}$ possibilities for an optimal solution, where $dim(q)$ stands for the dimension of the q. Instead, we search only $g_p \times k_p \times \dim(q)$ possibilities for a suboptimal solution and make the implementation of such an algorithm feasible.

After passing the signal through parallel-to-serial (P/S), digital-to-analog (DAC) conversion, and HPA, $\underline{\mathbf{x}}$ is sent through a frequency-selective Rayleigh fading channel. The impulse response of this channel is given as $\mathbf{h} = [h(1)...h(\upsilon)]^T$ where $h(\boldsymbol{\gamma}), \gamma = 1,...,\upsilon$ are circularly symmetric complex Gaussian random variables with $\mathcal{CN}(0, \frac{1}{\upsilon})$ distribution. With the assumption that the channel remains constant during the transmission of $\underline{\mathbf{x}}$ and L is sufficiently larger than υ, the received signal in frequency domain

$$\hat{y}(l) = \overline{h}(l)\hat{x}(l) + \overline{w}(l), \tag{2}$$

where $\hat{y}(l)$ denotes the received signal and the $\overline{w}(l)$ is the noise sample in the frequency domain. $\overline{h}(l)$ represents the channel fading coefficient at lth data tone. The distributions of $\overline{h}(l)$ and $\overline{w}(l)$ can be given by $\mathcal{CN}(0,1)$ and $\mathcal{CN}(0, \overline{\sigma}_0^2)$, respectively. $\overline{\sigma}_0^2$ is the noise variance in the frequency domain, whose time-domain relation can be written as $\overline{\sigma}_0^2 = \frac{K}{N}\sigma_0^2$. We define the SNR as $\rho = \frac{E_b}{\sigma_0}$, where $E_b = \frac{1}{R}\frac{N+L}{b}$ is the energy per bit.

2.2 | Coarse CFO estimator for H-OFDM-IM

In this section, we explain how the coarse CFO estimation can efficiently be performed based on the $g_p \times (n - k_p)$ null subcarriers in pilot subblocks.

After the time-domain signal is received by the receiver architecture in Figure 3, we perform serial-to-parallel (S/P) conversion and remove the CP. Once the CP is removed, the time-domain received signal can be represented as

$$\underline{y}(\iota) = \frac{K}{\sqrt{N}} \exp\left(\frac{j2\pi\epsilon_0\iota}{N}\right) \cdot \sum_{l \in \mathcal{A}} \hat{\alpha}(l) \cdot \exp\left(\frac{j2\pi l\iota}{N}\right) + w(\iota). \tag{3}$$

Algorithm 2 CFO search algorithm with golden ratio search

$\kappa,\ \Sigma,\ \xi,\ \delta,\ \underline{\mathbf{y}},\ K,\ N,\ \mathcal{Z}'$
$Z' \notin \emptyset,\ K \neq 0$
$\tau_1 \leftarrow \frac{\sqrt{5}-1}{2}$ ▷ Set τ_1 val. of. Golden R. Search
$\tau_2 \leftarrow 1 - \frac{\sqrt{5}-1}{2}$ ▷ Set τ_2 val. of. Golden R. Search
$x_1 \leftarrow \xi + \tau_2 \cdot (\delta - \xi)$ ▷ Calculate x_1
$x_2 \leftarrow \xi + \tau_1 \cdot (\delta - \xi)$ ▷ Calculate x_2
$x_{1q} \leftarrow \text{costfunc}(x_1,\ \underline{\mathbf{y}},\ \mathcal{Z}',\ K,\ N)$ ▷ Calculate cost value for x_1
$x_{2q} \leftarrow \text{costfunc}(x_2,\ \underline{\mathbf{y}},\ \mathcal{Z}',\ K,\ N)$ ▷ Calculate cost value for x_2
i $\leftarrow 1$ ▷ Repeat until max. iterations is reached
while i $< \kappa$ **do**
  if $|\delta - \xi| < \Sigma$ **then**
    break; ▷ If error is less than err. tolerance
  end if
  if $x_{1q} > x_{2q}$ **then**
    $\xi \leftarrow x_1$ ▷ Shrink search interval
    $x_1 \leftarrow x_2$
    $x_2 \leftarrow \xi + \tau_1 \cdot (\delta - \xi)$
    $x_{1q} \leftarrow x_{2q}$
    $x_{2q} = \text{costfunc}(x_2,\ \underline{\mathbf{y}},\ \mathcal{Z}',\ K,\ N)$ ▷ Calculate cost value for new x_2
  else
    $\xi \leftarrow x_2$ ▷ Shrink search interval
    $x_2 \leftarrow x_1$
    $x_1 \leftarrow \xi + \tau_2 \cdot (\delta - \xi)$
    $x_{2q} \leftarrow x_{1q}$
    $x_{1q} = \text{costfunc}(x_1,\ \underline{\mathbf{y}},\ \mathcal{Z}',\ K,\ N)$ ▷ Calculate cost value for new x_1
  end if
  i $\leftarrow$ i + 1 ▷ Increment iteration counter
end while
$\delta \leftarrow |x_{2q} - x_{1q}|$
$\hat{\epsilon} = \frac{\xi+\delta}{2}$ ▷ Calculate CFO estimation
return $\hat{\epsilon}$

Algorithm 3 Procedure costFunc

$\epsilon',\ \underline{\mathbf{y}},\ \mathcal{Z}',\ K,\ N$
$Z' \notin \emptyset,\ K \neq 0$
$\mathbf{D} \leftarrow \text{diag}([1, \exp(\frac{j2\pi\epsilon'}{N}), \ldots, \exp(\frac{j\cdot 2\pi\epsilon'(N-1)}{N})])$ ▷ Compute Matrix $\mathbf{D}$
$\hat{\mathbf{y}} \leftarrow \frac{\sqrt{K}}{N} \cdot \text{FFT}(\mathbf{D}^H \underline{\mathbf{y}})$ ▷ Compute FFT
return $|\hat{\mathbf{y}}(l)|^2,\ l \in \mathcal{Z}'$ ▷ Calculate cost calue

In (3), $\hat{\alpha}(l) = \overline{h}(l)\hat{x}(l)$ and $\hat{\alpha}(l)$ is the noise-free received signal in the frequency domain at the lth tone. ϵ_0 is the reference CFO value that is normalized to subcarrier spacing. Moreover, the vector representation of (3)

$$\underline{\mathbf{y}} = [\underline{y}(0), \underline{y}(1), ..., \underline{y}(N-1)]^T \tag{4}$$

and the vector of additive Gaussian noise samples in time can be expressed as

$$\mathbf{w} = [w(0), w(1), ..., w(N-1)]^T. \tag{5}$$

Furthermore, (4) can be also expressed in vector form as[17,23,24]

$$\underline{\mathbf{y}} = \mathbf{D}(\epsilon_0)\boldsymbol{\Phi}_{A'}\hat{\boldsymbol{\alpha}} + \mathbf{w}, \tag{6}$$

where

$$\begin{aligned}
&\mathbf{D}(\epsilon_0) = \mathrm{diag}\left(\left[1, \exp\left(\frac{j2\pi\epsilon_0}{N}\right), ..., \exp\left(\frac{j2\pi\epsilon_0(N-1)}{N}\right)\right]\right),\\
&\boldsymbol{\Phi}_{\mathcal{A}'} = \frac{\sqrt{K}}{N} \cdot [\boldsymbol{\phi}_{m_1}, \boldsymbol{\phi}_{m_2}, ..., \boldsymbol{\phi}_{m_K}], m_l \in \mathcal{A}',\\
&\boldsymbol{\phi}_{m_l} = [1, \exp(\tfrac{j2\pi m_l}{N}), ..., \exp(\tfrac{j2\pi m_l(N-1)}{N})]^T,\\
&\hat{\boldsymbol{\alpha}} = [\alpha(l_1), \alpha(l_2), ..., \alpha(l_K)]^T.
\end{aligned} \tag{7}$$

In (6), $\mathbf{D}(\epsilon_0)$ represents a diagonal matrix, and $\boldsymbol{\Phi}_{\mathcal{A}'}$ denotes an $N \times K$ sized matrix constructed with the active data tone indices of the received signal. Moreover, $\hat{\boldsymbol{\alpha}}$ is the vector form of the received frequency-domain signal excluded from the noise component. At this stage at the receiver, we perform a two-step CFO estimation and compensation. First, we estimate the CFO coarsely over the preassigned null subcarriers in the pilot subgroups. Second, we perform an index demodulation to detect the inactive data tones in the standard subblocks. Over these inactive data tones and null subcarriers, we perform a fine CFO estimation followed by a CFO compensation operation. The coarse CFO estimation over (6) with the knowledge of A'_p can be expressed as one-dimensional optimization problem[23,24]

$$\widehat{\epsilon_c} = \arg\max_{\epsilon} q_c(\epsilon), \tag{8}$$

where

$$q_c(\epsilon) = \underline{\mathbf{y}}^H \mathbf{D}(\epsilon)\boldsymbol{\Psi}_{A'_p}\mathbf{D}^H(\epsilon)\underline{\mathbf{y}}. \tag{9}$$

The maximum likelihood (ML) estimator in (8) estimates ϵ_0, where $\boldsymbol{\Psi}_{\mathcal{A}'_p} = \boldsymbol{\Phi}_{\mathcal{A}'_p}\boldsymbol{\Phi}^H_{\mathcal{A}'_p}$. With the estimated value $\hat{\epsilon}_c$ of ϵ_0, we can compensate the CFO coarsely. After coarse compensation, the received signal in time domain becomes

$$\underline{y}_c(\iota, \hat{\epsilon}_c) = \frac{\sqrt{K}}{N} e^{\frac{j2\pi(\epsilon_0 - \hat{\epsilon}_c)\iota}{N}} \cdot \sum_{l \in A'_p} \hat{\alpha}(l) \cdot e^{\frac{j2\pi l\iota}{N}} + w(\iota), \tag{10}$$

where the term $\epsilon_0 - \hat{\epsilon}_c$ is the coarse CFO estimation error. Equation (10) in vector form can be denoted by

$$\underline{\mathbf{y}}_c = \mathbf{D}^H(\hat{\epsilon}_c)\underline{\mathbf{y}}. \tag{11}$$

Here, the average MSE can be expressed as $E\{(\epsilon_0 - \widehat{\epsilon_c})^2\}$. Since this optimization problem consists of multiple minimas, the search algorithm must be designed carefully. The proposed search algorithm in Algorithms 2 and 3 is based on the golden ratio search algorithm, and it is capable of finding the global minima. κ, Σ, ξ, δ in Algorithms 2 and 3 correspond to the maximum number of iterations, error tolerance, and search interval upper and lower bounds, respectively. In Algorithm 3, ϵ' is the estimated CFO value in the ith iteration.

2.3 | Fine CFO estimator for H-OFDM-IM

In this section, we explain how the fine CFO estimation can efficiently be performed based $N - K$ active subcarriers in a H-OFDM-IM symbol.

The fine CFO estimator utilizes the inactive data tones generated by IM in combination with the preassigned null subcarriers in pilot subblocks. As a result the CFO estimation is greatly enhanced due to the increase in frequency diversity and samples. However, these inactive data tone indices are unknown at the receiver. To detect the inactive data tones, a series of operations must be performed. These operations begin with a FFT operation on (10):

$$\hat{y}_c = \frac{\sqrt{K}}{N}\mathrm{FFT}\{\underline{\mathbf{y}}_\mathbf{c}\} = \sqrt{K}\mathbf{F}_N\underline{\mathbf{y}}_\mathbf{c}. \tag{12}$$

Once the frequency-domain signal is obtained, we deinterleave the frequency-domain signal in (12) to obtain $\overline{\mathbf{y}}_c$, where $\overline{\mathbf{y}}_c$ has the H-OFDM-IM symbol structure given in Figure 1. At this stage, we rely on the low-complexity ML detector in Basar et al[24] to detect all inactive data tones in the signal. To detect these inactive data tones, we calculate the following:

$$\lambda(l) = \frac{|\overline{y}_c(l)|^2}{\overline{\sigma}_0^2} + \ln\left(\sum_{s_\chi \in \mathcal{S}} e^{-\frac{1}{\overline{\sigma}_0^2}|\overline{y}_c(l) - \overline{h}(l)s_\chi|^2)}\right). \tag{13}$$

In (13), $\lambda(l)$ is the log-likelihood ratio (LLR) value for each subcarrier in a given subblock, and l denotes the lth frequency index of the received signal. Therefore, $\overline{y}_c(l)$ stands for the samples in the frequency domain. Moreover, $s_\chi \in \mathcal{S}$ and $\mathcal{S}$ is the set of all M-ary constellation symbols. For BPSK modulation, (13) can be written as

$$\lambda(l) = \max(a,b) + \ln(1 + e^{-|b-a|}) + \frac{|\overline{y}_c(l)|^2}{\overline{\sigma}_0^2}, \tag{14}$$

where $a = \frac{-|\overline{y}_c(l) - \overline{h}(l)|^2}{\overline{\sigma}_0^2}$ and $b = \frac{-|\overline{y}_c(l) + \overline{h}(l)|^2}{\overline{\sigma}_0^2}$. After calculating the LLR value for each subcarrier in a given subblock, we construct the set $\mathcal{L} = \{\lambda(l_1), ..., \lambda(l_n)\}$. Then, we order the set $\mathcal{L}$ in ascending order to obtain $\mathcal{L}'$. From the set $\mathcal{L}'$, we select the first k_s elements, which we denote as $\mathcal{D} = \{d_1, d_2, ..., d_{k_s}\}$ for a standard subblock, where $\mathcal{D} \subset \mathcal{L}'$. $\mathcal{D}$ identifies the active and inactive subcarriers in a given standard subblock; therefore, we can estimate $\mathcal{A}$ and $\mathcal{Z}$ with $\mathcal{A}_f$ and $\mathcal{Z}_f$. By rearranging these indices, we can determine $\mathcal{A}'_f$ and $\mathcal{Z}'_f$.

At this stage, fine CFO estimation can be done on the time-domain signal in (1). The process of fine estimating the CFO value utilizes the same calculations in (5) and (6) and Algorithms 2 and 3 by replacing $\mathcal{A}'_p$ with $\mathcal{A}'_f$. The fine CFO estimation can be performed as follows:

$$\widehat{\epsilon_f} = \arg\max_{\epsilon} q_f(\epsilon), \tag{15}$$

and its cost function is

$$q_f(\epsilon) = \underline{\mathbf{y}}^H \mathbf{D}(\epsilon) \boldsymbol{\Psi}_{\mathcal{A}'_f} \mathbf{D}^H(\epsilon) \underline{\mathbf{y}}. \tag{16}$$

In (16), $\boldsymbol{\Psi}_{\mathcal{A}'_f} = \boldsymbol{\Phi}_{\mathcal{A}'_f} \boldsymbol{\Phi}^H_{\mathcal{A}'_f}$. After the fine CFO compensation, the received signal in time domain becomes

$$\underline{y}_f(\iota, \hat{\epsilon}_f) = \frac{\sqrt{K}}{N} e^{\frac{j2\pi(\epsilon_0 - \hat{\epsilon}_f)\iota}{N}} \cdot \sum_{l \in \mathcal{A}'_f} \hat{\alpha}(l) \cdot e^{\frac{j2\pi l \iota}{N}} + w(\iota), \tag{17}$$

where $\epsilon_0 - \hat{\epsilon}_f$ is the fine CFO estimation error. The average MSE can be expressed as $E\{(\epsilon_0 - \hat{\epsilon}_f)^2\}$. Equation (17) can be written in vector form as

$$\underline{\mathbf{y}}_f = \mathbf{D}^H(\hat{\epsilon}_f) \underline{\mathbf{y}}. \tag{18}$$

At the final stage of the CFO estimation, FFT and deinterleaving operations are necessary. The FFT operation can be given as

$$\hat{\mathbf{y}}_f = \frac{\sqrt{K}}{N} \mathrm{FFT}\{\underline{\mathbf{y}}_\mathbf{f}\} = \sqrt{K} \mathbf{F}_N \underline{\mathbf{y}}_\mathbf{f}, \tag{19}$$

where it converts the time-domain signal in (17) into a frequency-domain signal. After deinterleaving the frequency-domain signal $\hat{\mathbf{y}}_f$, demodulation can be performed on the resulting signal $\overline{\mathbf{y}}_f$. For the index demodulation, we follow (14) by replacing $\overline{\mathbf{y}}_c$ with $\overline{\mathbf{y}}_f$.

2.4 | SNR estimation for H-OFDM-IM

In this section, we explain how the SNR estimation can be precisely done based on the residual power on $N - K$ inactive subcarriers in a H-OFDM-IM symbol.

Once the indices of the active data tones are detected, the M-ary demodulation can be performed on the signal. Since proposed system adapts its modulations based on the channel quality in terms of SNR. It becomes vital to estimate the SNR at the receiver. This SNR estimation can be performed from the noise power on the null subcarrier indices. This SNR estimation can be denoted as

$$\hat{\rho} = \frac{E_b}{\frac{\sum_{z \in \mathcal{Z}_f} |y(z)|^2}{|\mathcal{Z}_f|}}, \tag{20}$$

where z denotes the inactive data tone indices in $\mathcal{Z}_f$ and $\hat{\rho}$ is the estimation of ρ. Obviously, (20) will be erroneous due to the presence of the CFO and therefore the ICI. There are some power leaks on to the inactive data tones due to the CFO estimation errors at the receiver. However, the equation in (20) can be modified to be more precise:

$$\hat{\rho}' = \frac{E_b}{\frac{\sum_{z \in \mathcal{Z}_f} |y(z)|^2}{|\mathcal{Z}_f|}} - C. \tag{21}$$

In (21), C is a positive correction factor constant and calculated by $C = \hat{\rho} - \rho$, which can be determined by mathematical calculations or computer simulations. Moreover, according to our computer simulation, C is a function of $|\mathcal{Z}_f|$ and therefore k_s, k_p, and g_p as well. Additionally, the SNR estimation error $|\rho - \hat{\rho}'|$ occurs due to the difference across time-domain and frequency-domain noise differences in OFDM-based systems.

3 | PERFORMANCE ANALYSIS OF H-OFDM-IM

In this section, we investigate the PAPR reduction performance, spectral efficiency and BER, bias and the MSE performance of the CFO estimation, and SNR estimation performance of the proposed H-OFDM-IM system. Additionally, we briefly discuss LDPC codes in general.

3.1 | Spectral efficiency

The spectral efficiency of the proposed system depends on the estimated received SNR $\hat{\rho}$, since the system parameters (coding rate [R], modulation order [M], etc.) are adjusted according to $\hat{\rho}$. By selecting different waveform parameters, we can optimize the spectral efficiency of H-OFDM-IM system for a given channel condition. For high SNR values, we let the system to operate with higher spectral efficiency values by changing the coding rate and k_s and M. To preserve BER performance, we increase the redundancy of proposed system under low SNR conditions by decreasing M and increasing k_p and k_s. The spectral efficiencies for different H-OFDM-IM configuration in comparison to conventional OFDM-IM and classical OFDM are given in Table 2.

3.2 | Fine CFO estimation

In this subsection, we derive the mathematically $E\{\widehat{\epsilon_f}\}$ and MSE of fine CFO estimation.

The analytical calculation of the CFO estimator's MSE can be calculated with the help of (15) and (16). For analytical MSE derivation of the fine CFO estimation, we assume that all inactive and active data tones are identified correctly. In other words, we consider the case where $\mathcal{A}'_f = \mathcal{A}'$. The expectation of the fine CFO estimate and its MSE can be approximated as[25,26]

$$E\{\hat{\epsilon}_f\} \approx \epsilon - \frac{E\{\dot{q}_f(\epsilon)\}}{E\{\ddot{q}_f(\epsilon)\}} MSE\{\hat{\epsilon}_f\} \approx \frac{E\{[\dot{q}_f(\epsilon)]^2\}}{[E\{\ddot{q}_f(\epsilon)\}]^2}, \tag{22}$$

where the $\dot{q}_f(\epsilon)$ and $\ddot{q}_f(\epsilon)$ are the first and the second derivatives of $q(\epsilon)$, where $\dot{q}_f(\epsilon)$ and $\ddot{q}_f(\epsilon)$ are

$$\begin{aligned}\dot{q}_f(\epsilon) = &\frac{j2\pi}{N}[\boldsymbol{\alpha}^H \boldsymbol{\Phi}^H_{\mathcal{A}'_f}(\mathbf{R}\boldsymbol{\Psi}_{\mathcal{A}'_f} - \boldsymbol{\Psi}_{\mathcal{A}'_f}\mathbf{R})\boldsymbol{\Phi}_{\mathcal{A}'_f}\boldsymbol{\alpha} \\ &+\boldsymbol{\alpha}^H \boldsymbol{\Phi}^H_{\mathcal{A}'_f}(\mathbf{R}\boldsymbol{\Psi}_{\mathcal{A}'_f} - \boldsymbol{\Psi}_{\mathcal{A}'_f}\mathbf{R})(\mathbf{D}^H(\epsilon)\mathbf{w}) + (\mathbf{D}^H(\epsilon)\mathbf{w})^H(\mathbf{R}\boldsymbol{\Psi}_{\mathcal{A}'_f} \\ &-\boldsymbol{\Psi}_{\mathcal{A}'_f}\mathbf{R})\boldsymbol{\Phi}_{\mathcal{A}'_f}\boldsymbol{\alpha} + (\mathbf{D}^H(\epsilon)\mathbf{w})^H(\mathbf{R}\boldsymbol{\Psi}_{\mathcal{A}'_f} - \boldsymbol{\Psi}_{\mathcal{A}'_f}\mathbf{R})(\mathbf{D}^H(\epsilon)\mathbf{w})],\end{aligned} \tag{23}$$

TABLE 2 Spectral efficiency of H-OFDM-IM system (with eight pilot subblocks), conventional OFDM-IM (without any CFO estimation over null subcarriers), and classical OFDM (with 128 null subcarriers, 32 preknown null subcarriers, and 96 unknown null subcarriers)

Scheme	$R=\frac{1}{2}$ (bits/Hz/s)	$R=\frac{2}{3}$ (bits/Hz/s)	$R=\frac{4}{5}$ (bits/Hz/s)	$R=\frac{8}{9}$ (bits/Hz/s)
H-OFDM-IM $(k_s,M)=(4,2)$	0.18	0.24	0.28	0.31
H-OFDM-IM $(k_s,M)=(4,4)$	0.35	0.47	0.56	0.63
OFDM-IM $(n,k,M)=(8,4,2)$	0.59	0.78	0.94	1.05
OFDM-IM $(n,k,M)=(8,4,4)$	0.82	1.10	1.32	1.46
OFDM $(nSC,M)=(32+96,2)$	0.14	0.19	0.23	0.25
OFDM $(nSC,M)=(32+96,4)$	0.29	0.38	0.46	0.51

$$\begin{aligned}\ddot{q}_f(\epsilon) = &\frac{4\pi^2}{N^2}[\boldsymbol{\alpha}^H \boldsymbol{\Phi}^H_{\mathcal{A}'_f}(2\mathbf{R}\boldsymbol{\Psi}_{\mathcal{A}'_f}\mathbf{R} - \boldsymbol{\Psi}_{\mathcal{A}'_f}\mathbf{R}^2 - \mathbf{R}^2\boldsymbol{\Psi}_{\mathcal{A}'_f})\boldsymbol{\Phi}_{\mathcal{A}'_f}\boldsymbol{\alpha} \\ &+\boldsymbol{\alpha}^H \boldsymbol{\Phi}^H_{\mathcal{A}'_f}(2\mathbf{R}\boldsymbol{\Psi}_{\mathcal{A}'_f}\mathbf{R} - \boldsymbol{\Psi}_{\mathcal{A}'}\mathbf{R}^2 - \mathbf{R}^2\boldsymbol{\Psi}_{\mathcal{A}'_f})(\mathbf{D}^H(\epsilon)\mathbf{w}) \\ &+(\mathbf{D}^H(\epsilon)\mathbf{w})^H(2\mathbf{R}\boldsymbol{\Psi}_{\mathcal{A}'_f}\mathbf{R} - \boldsymbol{\Psi}_{\mathcal{A}'_f}\mathbf{R}^2 - \mathbf{R}^2\boldsymbol{\Psi}_{\mathcal{A}'_f})\boldsymbol{\Phi}_{\mathcal{A}'_f}\boldsymbol{\alpha} \\ &+(\mathbf{D}^H(\epsilon)\mathbf{w})^H(2\mathbf{R}\boldsymbol{\Psi}_{\mathcal{A}'_f}\mathbf{R} - \boldsymbol{\Psi}_{\mathcal{A}'_f}(\mathbf{R})^2 - \mathbf{R}^2\boldsymbol{\Psi}_{\mathcal{A}'_f})(\mathbf{D}^H(\epsilon)\mathbf{w})].\end{aligned} \tag{24}$$

Here, $\mathbf{R} = \text{diag}(0,1,...,N-1)$ and $\mathbf{y}$ is given in (8). Since $\mathbf{w}$ is a zero mean additive Gaussian noise vector with $\mathcal{CN}(0,\overline{\sigma}_0^2)$ and $E\{\mathbf{w}\} = 0$, the terms in (23) and (24), which contain $\mathbf{w}$ or any linear combination of $\mathbf{w}$, vanish. As a result, we can rewrite (23):

$$E\{\dot{q}_f(\epsilon)\} = \frac{j2\pi}{N}[\boldsymbol{\alpha}^H \boldsymbol{\Phi}^H_{\mathcal{A}'_f}(\mathbf{R}\boldsymbol{\Psi}_{\mathcal{A}'_f} - \boldsymbol{\Psi}_{\mathcal{A}'_f}\mathbf{R})\boldsymbol{\Phi}_{\mathcal{A}'_f}\boldsymbol{\alpha} + \sigma_0^2\mathbf{I}]. \tag{25}$$

Similarly for (25), we end up with

$$\begin{aligned}E\{\ddot{q}_f(\epsilon)\} = &\frac{4\pi^2}{N^2}[\boldsymbol{\alpha}^H \boldsymbol{\Phi}^H_{\mathcal{A}'_f}(2\mathbf{R}\boldsymbol{\Psi}_{\mathcal{A}'_f}\mathbf{R} - \boldsymbol{\Psi}_{\mathcal{A}'_f}\mathbf{R}^2 \\ &-\mathbf{R}^2\boldsymbol{\Psi}_{\mathcal{A}'_f})\boldsymbol{\Phi}_{\mathcal{A}'_f}\boldsymbol{\alpha} + \sigma_0^2\mathbf{I}].\end{aligned} \tag{26}$$

Both of these terms are deterministic, under the assumption that no false alarm occurred, in other words, all inactive data tones are determined successfully, $\dot{q}_f(\epsilon) = 0$. As a result, an unbiased estimator $E\{\hat{\epsilon}_f\} = \epsilon_0$ is reached. Finally, $E\{\hat{\epsilon}_f\} = \epsilon_0$ holds for the high SNR values in which no false alarm occurs. Then, (26) can be rewritten as

$$E\{\ddot{q}_f(\epsilon)\} = \frac{4\pi^2}{N^2}\boldsymbol{\alpha}^H \boldsymbol{\Phi}^H_{\mathcal{A}'_f}\mathbf{V}_2\Phi_{\mathcal{A}'_f}\boldsymbol{\alpha}, \tag{27}$$

where $\mathbf{V}_2 = 2\mathbf{R}\boldsymbol{\Psi}_{\mathcal{A}'_f}\mathbf{R} - \boldsymbol{\Psi}_{\mathcal{A}'_f}\mathbf{R}^2 - \mathbf{R}^2\boldsymbol{\Psi}_{\mathcal{A}'_f}$. Moreover, from (27), we have

$$E\{[\dot{q}_f(\epsilon)]^2\} = \frac{-4\pi^2}{N^2}(2\overline{\sigma}_0^2\boldsymbol{\alpha}^H \boldsymbol{\Phi}^H_{\mathcal{A}'_f}\mathbf{V}_1\mathbf{V}_1\boldsymbol{\Phi}_{\mathcal{A}'_f}\boldsymbol{\alpha}) + [\mathbf{w}^H\mathbf{V}_1\mathbf{w}]^2. \tag{28}$$

From (27) and (28), MSE in the (22) becomes

$$MSE\{\hat{\epsilon}_f\} \approx \frac{N^2 2\overline{\sigma}_0^2\boldsymbol{\alpha}^H \boldsymbol{\Phi}^H_{\mathcal{A}'_f}\mathbf{V}_1\mathbf{V}_1\Phi_{\mathcal{A}'_f}\boldsymbol{\alpha}}{4\pi^2[\boldsymbol{\alpha}^H \boldsymbol{\Phi}^H_{\mathcal{A}'_f}\mathbf{V_2}\boldsymbol{\Phi}_{\mathcal{A}'_f}\boldsymbol{\alpha}]^2}, \tag{29}$$

where $\mathbf{V}_1 = \mathbf{R}\boldsymbol{\Psi}_{\mathcal{A}'_f} - \boldsymbol{\Psi}_{\mathcal{A}'_f}\mathbf{R}$. In (29), we express the MSE in the CFO estimation analytically under the condition that all of the inactive data tones are detected correctly at the receiver.

3.3 | LDPC codes

In this section, we provide a brief discussion about LDPC codes, which we have considered as a forward error correction code (FEC) for the simulation of proposed H-OFDM-IM system.

LDPC codes are linear block codes, whose parity check matrix is defined as a sparse one. The LDPC codes attracted much attention in last two decades due to their near Shannon limit performances. Despite high complexity and considerable latency of LDPC codes, they are widely used in modern communication systems such as 5G due to their easy implementation in hardware. Moreover, LDPC codes in comparison to Turbo codes provide superior coding gain when the code length is sufficient, easy implementation, great flexibility, and theoretical verifiability. Since we designed

H-OFDM-IM system around robustness, we considered using LDPC codes used in the DVB-S2 long frame structure. Overall, with the introduction of the LDPC codes, we can achieve superior error correction capabilities at the receiver in the expense of latency.

4 | SIMULATION AND PERFORMANCE RESULTS OF H-OFDM-IM SYSTEM

In this section, we present our computer simulation results for the H-OFDM-IM scheme. First, in this section, we analyze the PAPR reduction performance of proposed H-OFDM-IM scheme with classical OFDM and conventional OFDM-IM. Second, we provide the SNR estimation $\hat{\rho}'$ performance with respect to $\hat{\rho}$. Then, we provide the MSE in CFO estimation for H-OFDM-IM and classical OFDM-IM. Lastly, we compare the BER performance of H-OFDM-IM with classical OFDM under normalized CFO $\epsilon = 0.4$ and under LDPC codes with respect to the DVBS-2 standards. Then, we briefly discuss the thresholds to change the modulation order, coding rate, and therefore, the spectral efficiency of the system with respect to estimated SNR $\hat{\rho}'$, in an adaptive way.

For the simulation, we consider a subblock size $n = 8$ and $k_p = 4$ for which pilot indices can be selected as $\{1, 3, 5, 7\}$ or $\{2, 4, 6, 8\}$. For standard subblocks, we select either k_s as $k_s = 4$ or $k_s = 2$ depending on the channel conditions. Further simulation parameters are given in Table 3.

For modulation order M, we consider only BPSK and QPSK for our simulations, since these are the most robust modulation schemes, still used in the modern communication systems such as 5G. However, we would also like to note that higher order modulation schemes can also be used to achieve better spectral efficiency rates if the channel conditions are sufficient for them.

In Figure 4, we analyze the performance of proposed low-complexity PAPR reduction algorithm, which does not require any side information. As a result, no processing is required at the receiver, which reduces the complexity of the system. Moreover, to obtain optimal PAPR values, an optimal algorithm has to calculate $C(g_p \times k_p \times \dim(q), g_p \times k_p) = \frac{(g_p \times k_p \times dim(q))!}{(g_p \times k_p)!((\dim(q)-1) \times g_p \times k_p)!}$ different PAPR values and compare them. Therefore, the complexity of the optimal PAPR reduction algorithm is upper bounded by $\mathcal{O}((g_p \times k_p)!)$. However, proposed suboptimal low-complexity PAPR reduction algorithm calculates only $g_p \times k_p \times \dim(q)$ different PAPR values, which is upper bounded by $\mathcal{O}(g_p \times k_p)$. By only using $g_p \times k_p = 16$ active data tones in g_p pilot subblocks, we compare proposed scheme with the conventional OFDM-IM and classical OFDM. As seen from Figure 4, we can achieve around 3- to 4-dB PAPR reduction. In comparison to classical OFDM-IM with $n = 4$ subcarriers per subblock and $k = 2$ active subcarriers per subblock, we achieve more than 3- to 4-dB PAPR reduction. Moreover, in comparison to classical OFDM, we achieve again 3- to 4-dB PAPR reduction. Obviously, proposed PAPR reduction algorithm is not the optimal one; however, keeping the PAPR algorithm simple and removing the necessity of sending side information contributes positively to the spectral efficiency of the H-OFDM-IM system. Additionally, in comparison to conventional OFDM-IM and classical OFDM, proposed system is much less likely to operate in HPA's nonlinear region. Therefore, it is less likely to experience distortion caused by the HPA.

In Figure 5, we analyze coarse and fine CFO estimation performance of proposed system in comparison to the classical OFDM. In this comparison, we did not include the conventional OFDM-IM, since to make a fair comparison, we have to introduce null subcarrier to an OFDM-IM symbol, which would result in designing another waveform and would be out of scope of this paper. However, by introducing same amount of null subcarriers as we have considered for proposed H-OFDM-IM symbol, $g_p \times (n - k_p)$ null subcarriers to classical OFDM, we can make a fair comparison. As seen from Figure 5, we can achieve a better CFO estimation MSE for proposed H-OFDM-IM symbol in comparison to the classical OFDM with $g_p \times (n - k_p)$ null subcarriers, due to utilization of inactive data tones generated by the IM in standard subblocks. However, it is important to note that classical OFDM with $g_p \times (n - k_p)$ null subcarriers and coarse CFO estimation method of proposed H-OFDM-IM systems gives better MSE results under low SNR conditions. This is somewhat expected, since under low SNR conditions, ML IM decoder at the receiver is likely to make errors in estimation of active and inactive data tones in standard subblocks and therefore disturbs the fine CFO estimation. For high SNR conditions, we can see that in Figure 5, we can reach the theoretical limits for both coarse and fine CFO estimation as we have driven in previous sections in this paper. The slight mismatch with the theoretical expectations and the simulation results comes from the iteration and precision limits that we have included in the Algorithms 1 and 2 to keep the latency considerably low. Furthermore, we see that the more null subcarriers and the more inactive data tones present in the H-OFDM-IM waveform provides a better CFO estimation, due to the increased samples at the receiver. As a conclusion of Figure 5, CFO can be estimated in an unbiased way for proposed H-OFDM-IM scheme, and proposed scheme can efficiently operate even in high CFO ($\epsilon = 0.4$) scenarios. Therefore, our work has revealed that

TABLE 3 Computer simulation parameters of H-OFDM-IM system

Simulation parameters	Notation	Value
Number of subcarriers	N	256
Cyclic prefix length	L	16 samples
Number of subcarriers per subblocks	n	8
Number of active subcarriers per pilot subblocks	k_p	4
Number of active subcarriers per standard subblocks	k_s	{2, 4}
Number of subblocks per OFDM-IM symbol	g	32
Number of pilot subblocks per OFDM-IM symbol	g_p	4 or 8
Number of standard subblocks per OFDM-IM symbol	g_s	28
M-ary modulations	M	BPSK,QPSK
Number of Rayleigh channel taps	h_r	10
CFO value normalized to subcarrier spacing	ϵ	0.4
LDPC encoder code block length	m_c	64,800 bits
LDPC encoder coding rate	R	{1/2, 2/3, 8/10, 8/9}

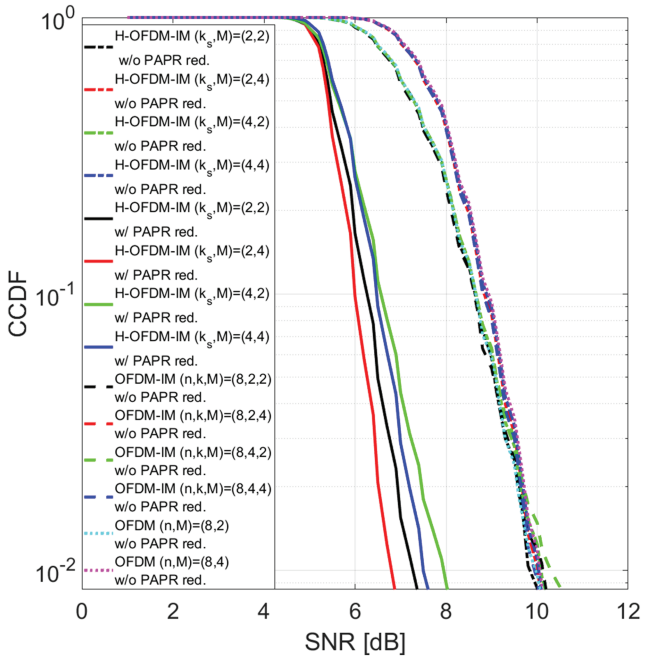

FIGURE 4 PAPR reduction performance of H-OFDM-IM system (with $g_p = 4$), PAPR of conventional OFDM-IM, and PAPR of classical OFDM

H-OFDM-IM can be an alternative for OFDM in future systems which require robust operation with low PAPR and in the presence of high CFO.

In Figure 6, we provide the estimated SNR values for different H-OFDM-IM configurations. As in the CFO estimation, due different number of null subcarriers and inactive data tones in an H-OFDM-IM symbol, we get different SNR estimation results. The more inactive data tones present in an H-OFDM-IM symbol, the more erroneous is the SNR estimation. This is somewhat counterintuitive at first. However, this behavior can be explained by the time and frequency-domain noise level mismatches in OFDM-based systems. This offset behavior of SNR estimation can easily be compensated with a constant C, as explained in previous sections. The corrected SNR estimations have significantly lower error rates, especially for high SNR scenarios, where the ML estimator can detect the null subcarriers in standard subblocks. As a conclusion, we can estimate SNR precise enough to send feedback information to the receiver to change the IM,

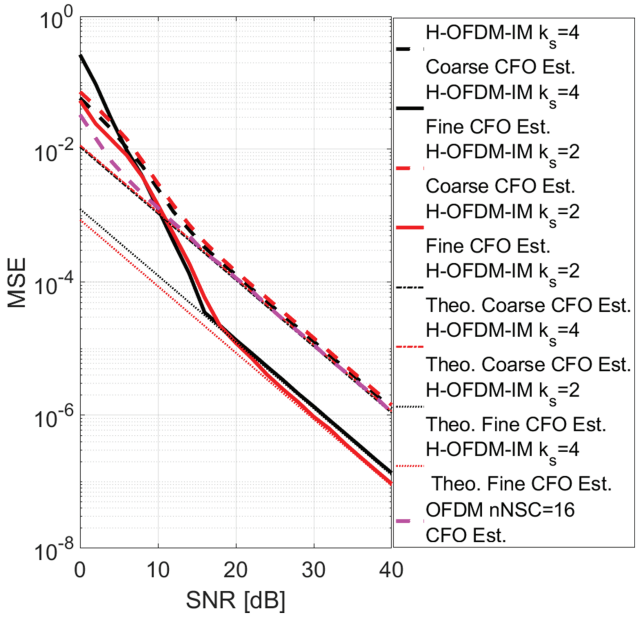

FIGURE 5 MSE performance of coarse and fine CFO estimation of H-OFDM-IM system (with $g_p = 4$) and classical OFDM with 16 preknown null subcarriers under $\epsilon = 0.4$

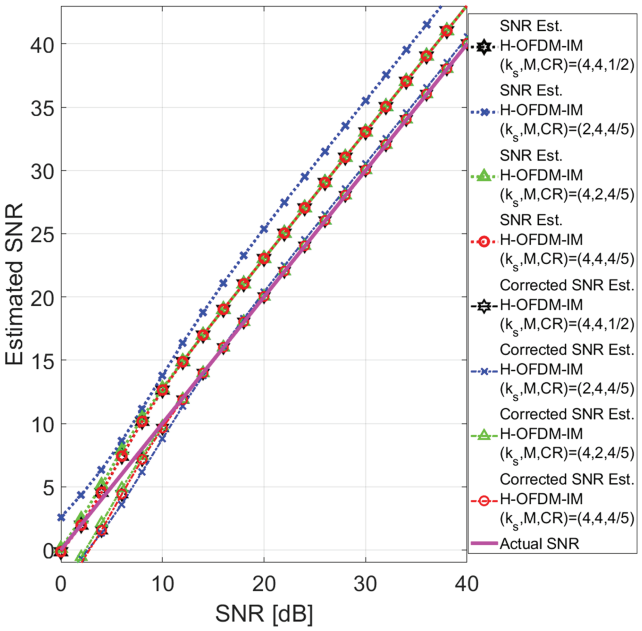

FIGURE 6 SNR estimation of H-OFDM-IM system (with $g_p = 4$) under $\epsilon = 0.4$

modulation order and R. Moreover, we can efficiently change the spectral efficiency of proposed system to operate more efficiently depending on the channel SNR.

In Figure 7, we compare the BER performance of H-OFDM-IM and classical OFDM with $g_p \times (n - k_p) + g_s \times (n - k_s)$ null subcarriers under $\epsilon = 0.4$ normalized CFO. Further to represent a fair CFO comparison, we utilize $g_p \times (n - k_p)$ preknown null subcarriers in OFDM for the CFO estimation. We would like to note that classical OFDM and conventional OFDM-IM without any CFO estimator and compensator would perform BER = 0.5 under $\epsilon = 0.4$. Here, we see that classical OFDM would outperform the H-OFDM-IM, due to lack of IM and better CFO compensation at low SNR rates. However, a classical OFDM waveform with null subcarriers cannot compete with proposed high-

diversity IM solution with unique SAPs, which can carry information with low BER under low SNR conditions. Despite that the proposed H-OFDM-IM system outperforms the classical OFDM with null subcarriers both in high SNR conditions and spectral efficiency. Further, we would like to emphasize that the information carried with IM in standard sub-blocks are not coded and therefore can be used directly to send information about the waveform (modulation order, coding rate, etc.) or can be used for any purpose depending on the application. Additionally, classical OFDM with some null subcarriers also lacks PAPR reduction, which may cause operation of HPAs in their nonlinear region and can cause amplitude-to-amplitude or amplitude-to-phase distortion of a symbol.

Lastly, in Figure 8, we share the determined threshold levels for the received SNR values. By looking at Figure 8, one can set the system parameters depending on the received feedback from the receiver. The thresholds can be selected depending on the desired BER level, which can obtained from Figure 7. For the case given in Figure 8, we considered 10^{-3} BER level to be sufficient for a voice communication channel and selected the SNR values depending on this scenario. As a result, a joint optimization of spectral efficiency, BER, PAPR, and CFO estimation performance can be achieved for proposed H-OFDM-IM scheme.

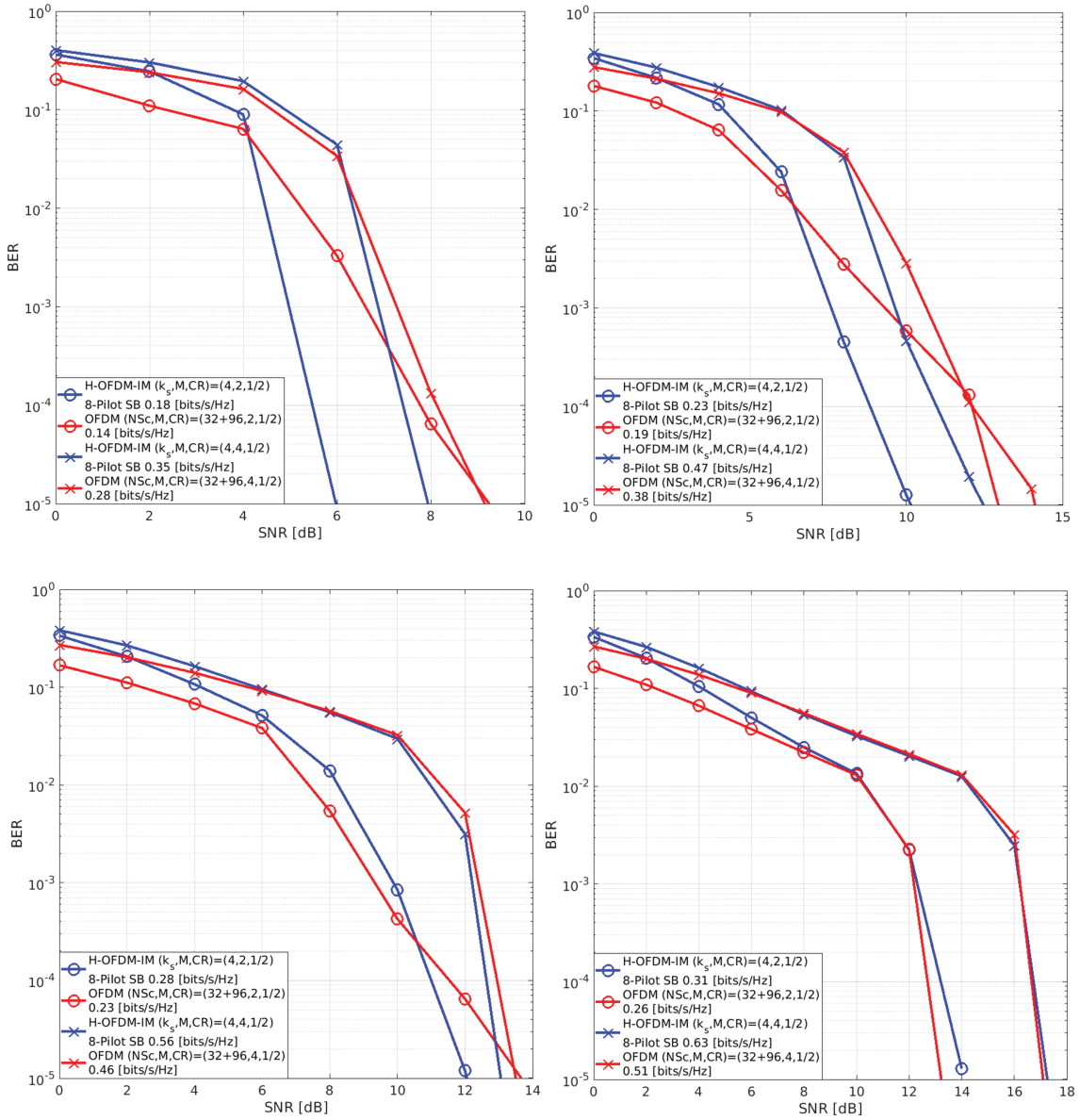

FIGURE 7 BER performance of H-OFDM-IM system (with $g_p = 8$) and classical OFDM with 128 null subcarriers (32 preknown and 96 unknown) under $\epsilon = 0.4$. (A) with $CR = R = \frac{1}{2}$. (B) with $CR = R = \frac{2}{3}$. (C) with $CR = R = \frac{8}{10}$. (D) with $CR = R = \frac{8}{9}$

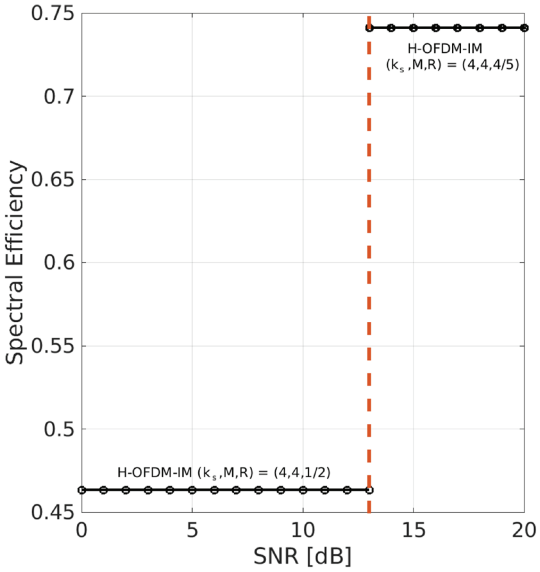

FIGURE 8 Spectral efficiency adaptation based on the received SNR of H-OFDM-IM system (with $g_p = 4$) with $\epsilon = 0.4$

5 | CONCLUSION

In this paper, we have proposed a reliable H-OFDM-IM waveform, which can reduce PAPR without sending a side information. Moreover, proposed system can estimate and compensate CFO precise enough and can efficiently estimate the received SNR value by taking the the power leakages into account, which occurs due to the errors in CFO estimation as well. As a conclusion, proposed system is capable of adjusting its IM architecture and code rate in an adaptive way, such that it can operate efficiently even in high CFO scenarios. Furthermore, the proposed system's ability to estimate CFO is validated with both simulation results and analytical derivations. Additionally, we have showed that the received SNR over inactive data tones can be efficiently estimated even in high SNR scenarios. Lastly, we have proven that, by sacrificing the spectral efficiency, we can achieve better BER performance by increasing the diversity gain in IM bits and optimizing the selection of these certain system parameters depending on the received SNR adaptively. The optimization of the LDPC decoder for the proposed H-OFDM-IM scheme remains to be considered as future work. The optimization of the LDPC decoder is expected to enhance the LDPC BER performance of the proposed H-OFDM-IM scheme quite significantly.

ACKNOWLEDGMENTS

This work is supported by ASELSAN A.S. with Grant HBT-TE-2019-010. Patent application is submitted to Turkish Patent & Trademark Office under Application Number 2020/20885.

DATA AVAILABILITY STATEMENT

The data that support the findings of this study are available from the corresponding author upon reasonable request.

REFERENCES

1. Başar E, Aygolu U, Panayirci E, Poor HV. Orthogonal frequency division multiplexing with index modulation. *IEEE Trans Signal Process*. 2013;61(22):5536-5549.
2. Başar E. OFDM with index modulation using coordinate interleaving. *IEEE Wirel Commun Lett*. 2015;4(4):381-384.
3. Wen M, Ye B, Basar E, Li Q, Ji F. Enhanced orthogonal frequency division multiplexing with index modulation. *IEEE Trans Wirel Commun*. 2017;16(7):4786-4801.
4. Wen M, Basar E, Li Q, Zheng B, Zhang M. Multiple-mode orthogonal frequency division multiplexing with index modulation. *IEEE Trans Commun*. 2017;65(9):3892-3906.
5. Khedkar AR, Admane P. Estimation and reduction of CFO in OFDM system. In: 2015 International Conference on Information Processing (ICIP); 2015:130-134.
6. Pollet T, Van Bladel M, Moeneclaey M. BER sensitivity of OFDM systems to carrier frequency offset and Wiener phase noise. *IEEE Trans Commun*. 1995;43(2/3/4):191-193.

7. Thota S, Kamatham Y, Paidimarry CS. Analysis of hybrid PAPR reduction methods of OFDM signal for HPA models in wireless communications. *IEEE Access*. 2020;8:22780-22791.
8. Wu J, Fan P. A survey on high mobility wireless communications: challenges, opportunities and solutions. *IEEE Access*. 2016;4:450-476.
9. Lin T, Phoong S. A low-complexity blind CFO estimation for OFDM systems. In: 2014 IEEE International Conference on Acoustics, Speech and Signal Processing (ICASSP); 2014:8083-8086.
10. Ren T, Zhang E. A simple blind CFO estimation algorithm for multi-user OFDM system. In: 2007 16th IST Mobile and Wireless Communications Summit; 2007:1-4.
11. Ramadan K, Dessouky MI, Abd El-Samie FE, Fiky AS. Equalization and blind CFO estimation for performance enhancement of OFDM communication systems using discrete cosine transform. *Int J Commun Syst*. 2020;33(3):e3984.
12. Besseghier M, Djebbar AB. Novel blind CFO estimation method for OFDM/OQAM system. *IEEE Commun Lett*. 2020;24(7):1451-1454.
13. Mokhtar B, Djebbar AB, Iyad D, Abdelmalik T. Joint semi-blind estimation of CFO and channel for OFDM system. In: 2014 International Conference on Electrical Sciences and Technologies in Maghreb (CISTEM); 2014:1-5.
14. Nishad PK, Singh P. Carrier frequency offset estimation in OFDM systems. In: 2013 IEEE Conference on Information Communication Technologies; 2013:885-889.
15. Lin T-T, Hwang F-H. Analysis and design of joint CFO/channel estimate techniques for a cooperative STBC-OFDM system. *Int J Commun Syst*. 2019;32(2):e3845.
16. Ma, X, Tepedelenlioglu C, Giannakis GB, Barbarossa S. Non-data-aided carrier offset estimators for OFDM with null subcarriers: identifiability, algorithms, and performance. *IEEE J Sel Areas Commun*. 2001;19(12):2504-2515.
17. Yang Z, Chen F, Zheng B, Wen M, Yu W. Carrier frequency offset estimation for OFDM with generalized index modulation systems using inactive data tones. *IEEE Commun Lett*. 2018;22(11):2302-2305.
18. Wang L, Xinghai Y, Yutai W. PTS scheme with low complexity IFFTs for PAPR reduction in SISO/MIMO OFDM. In: 2013 IEEE 4th International Conference on Electronics Information and Emergency Communication; 2013:181-184.
19. Liang H-Y. Selective mapping technique based on an adaptive phase-generation mechanism to reduce peak-to-average power ratio in orthogonal frequency division multiplexing systems. *IEEE Access*. 2019;7:96712-96718.
20. Thota S, Kamatham Y, Paidimarry CS. Analysis of hybrid PAPR reduction methods of OFDM signal for HPA models in wireless communications. *IEEE Access*. 2020;8:22780-22791.
21. Hosseinzadeh Aghdam M, Sharifi AA. A novel ant colony optimization algorithm for PAPR reduction of OFDM signals. *Int J Commun Syst*. 2021;34(1):e4648.
22. Memisoglu E, Basar E, Arslan H. Low complexity peak-to-average power ratio reduction in OFDM-IM. In: 2018 IEEE International Black Sea Conference on Communications and Networking (BlackSeaCom); 2018:1-5.
23. Ghogho M, Swami A, Giannakis GB. Optimized null-subcarrier selection for CFO estimation in OFDM over frequency-selective fading channels. In: GLOBECOM'01. IEEE Global Telecommunications Conference (Cat. No. 01CH37270), Vol. 1; 2001:202-2061.
24. Basar E, Aygolu U, Panayirci E. Orthogonal frequency division multiplexing with index modulation in the presence of high mobility. In: 2013 First International Black Sea Conference on Communications and Networking (BlackSeaCom); 2013:147-151.
25. Morelli M, Mengali U. Carrier-frequency estimation for transmissions over selective channels. *IEEE Trans Commun*. 2000;48(9):1580-1589.
26. So HC, Chan YT, Ho KC, Chen Y. Simple formulae for bias and mean square error computation [DSP tips and tricks]. *IEEE Signal Process Mag*. 2013;30(4):162-165.

How to cite this article: Erol Gurol I, Basar E, Kucukyavuz D, Atay Onat F. A novel orthogonal frequency division multiplexing with index modulation waveform with carrier frequency offset resistance and low peak-to-average power ratio. *Int J Commun Syst*. 2022;35(7):e5094. doi:10.1002/dac.5094